Observation of the Effects of Radially Sheared Electric Fields on the Suppression of Turbulent Vortex Structures and the Associated Transverse Loss in GAMMA 10

著者別名	小波藏 純子, 平田 真史, 沼倉 友晴, 市村 真, 片沼 伊佐夫, 吉川 正志, 今井 剛
journal or publication title	Physical review letters
volume	94
number	8
page range	085002
year	2005-03
権利	(C) 2005 The American Physical Society
URL	http://hdl.handle.net/2241/104161

doi: 10.1103/PhysRevLett.94.085002

Observation of the Effects of Radially Sheared Electric Fields on the Suppression of Turbulent Vortex Structures and the Associated Transverse Loss in GAMMA 10

T. Cho,[1] M. Yoshida,[1] J. Kohagura,[1] M. Hirata,[1] T. Numakura,[1] H. Higaki,[1] H. Hojo,[1] M. Ichimura,[1] K. Ishii,[1] K. Md. Islam,[1] A. Itakura,[1] I. Katanuma,[1] Y. Nakashima,[1] T. Saito,[1] Y. Tatematsu,[1] M. Yoshikawa,[1] Y. Kojima,[1] S. Tokioka,[1] N. Yokoyama,[1] Y. Tomii,[1] T. Imai,[1] V. P. Pastukhov,[2] S. Miyoshi,[1] and GAMMA 10 Group[1]

[1]*Plasma Research Center, University of Tsukuba, Tsukuba, Ibaraki 305-8577, Japan*
[2]*Russian Research Center "Kurchatov Institute," Moscow, Russia*
(Received 25 July 2004; published 3 March 2005)

Vortexlike turbulent structures in hot-ion mode plasmas with several keV are observed in the case with a radially produced weak shear of electric fields E_r. However, a strong E_r shear formation due to a high ion-confining potential ϕ_c production clears up these vortices together with plasma-confinement improvement and disappearance of both drift-wave and turbulencelike Fourier spectral signals. These findings are based on three-time progress in ϕ_c in comparison to ϕ_c attained 1992–2002. The significant advance of ϕ_c is well extended in line with proposed potential-formation physics scalings.

DOI: 10.1103/PhysRevLett.94.085002 PACS numbers: 52.55.Jd, 52.25.Fi, 52.35.Ra, 52.70.La

Experimental verification of the effects of the formation of radially sheared electric fields E_r (or potentials) in plasmas is one of the most critical issues to understand physics bases for plasma-confinement improvements found in various types of devices. One of the most essential and inherent characteristic advantages of open-ended mirror devices [1–9] is the ease of control of a radial potential distribution and the associated E_r shear profile or the frequency of a nonuniform sheared plasma rotation [$\Omega_r = E_r/(r_c B)$] profile. Such a control of Ω_r or E_r in mirror devices is easily carried out on the basis of driving axial fast electron flows from plug electron-cyclotron heating (ECH) regions [8,9] into open-ended mirror regions along the lines of magnetic force [8–13]. (Here, r_c denotes a radius mapped to the central cell.) Thus, the profile control of the axial electron flows due to ECH power control of the radial distribution and intensity (see below) provides a convenient "active control" method of the shear profile. This allows for flexible and advantageous mirror experiments for constructing common relations between the shear profiles and reductions in fluctuation-driven radial plasma losses (or transverse confinement) along with physics details of interior hot-plasma behavior.

Recently, three-time progress in the formation of ion-confining potentials ϕ_c including a record of 2.1 kV in the plug region (filled circles in Fig. 1), in comparison to ϕ_c attained 1992–2002 [14,15] (open circles in Fig. 1), is achieved in a hot-ion mode [14–17] having bulk-ion temperatures T_i = several keV. The advance in the potential formation leads to a finding of remarkable effects of sheared E_r (i.e., $E_r' = dE_r/dr \approx$ several 10 kV/m^2) or sheared Ω_r on the suppression of not only a coherent drift-wave-relevant Fourier component but also broadband turbulencelike fluctuations (or vortexlike structures; see below) in GAMMA 10. Here, the progress in the potential formation is made in line with the extension of our proposed scaling of ϕ_c with powers of plug ($P_{\rm PECH}$) and barrier ($P_{\rm BECH}$) ECH [14,15] (see the data fit to the scaling surface in Fig. 1) covering representative tandem-mirror operational modes, characterized in terms of a high-potential mode having kV-order plasma-confining potentials [5,8,9] and a hot-ion mode yielding fusion neutrons with T_i = 10–20 keV [17].

The progress of higher ϕ_c formation in turn gives bases for the following remarkable effects of the formation of a strong central cell E_r or Ω_r *shear,* since the shear is proportional to the central cell (Φ_C) and plug (Φ_P) potentials. Along the lines of magnetic force, Φ_C is closely connected with and raised by a Φ_P rise due to plug ECH having the Gaussian power-lobe profile of $P_{\rm ECH}(0) \times \{\exp[-(r_c/a)^2]\}$. In fact, such a proportionality of Φ_C to

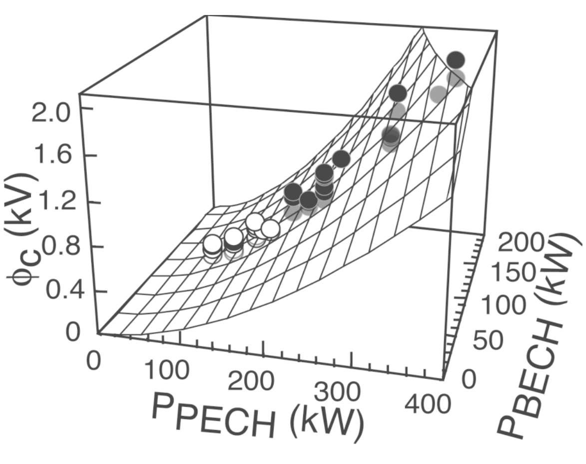

FIG. 1. Three-time advance in ϕ_c including a record of 2.1 kV (filled circles), in comparison to ϕ_c attained 1992–2002 (open circles), extensionally fits well to the scaling surface of ϕ_c with plug ($P_{\rm PECH}$) and barrier ($P_{\rm BECH}$) ECH powers (see Refs. [14,15]). Here, $n_c = 2 \times 10^{18}$ m^{-3} is exemplified for a tandem-mirror configuration with $n_p/n_c = 0.1$ and T_i = several keV.

Φ_P is experimentally observed [11,12]. Here, (0) indicates values at $r_c = 0$, and Φ and ϕ denote the absolute value and difference of potentials, respectively.

Nonuniform plasma rotation can suppress existing plasma instabilities and fluctuations. As a result, the considerable reduction of cross-field plasma transport is expected. Analyzing results of Ref. [18] and other aspects of the problem (in particular, see subsections 1.6.2 and 2.1.1 in Ref. [18]) provide the value $W_r = [\nabla \times (nV_E)]_z/n(0) = (nr_c^2\Omega_r)'/[n(0)r_c]$ (i.e., the z component of the normalized vorticity of plasma momentum density) as an appropriate measure of the $E \times B$ velocity (V_E) shear in the case of rotating plasmas with nonuniform density profiles. [For slab flows with a uniform density, $W_{\text{slab}-x} = dV_E/dx$, and $W_r = (2/B)[n/n(0)](dE_r/dr)$ for the cylindrical geometry having the same e-folding lengths of the Gaussian profiles for n and Φ_c.]

Here, we outline the GAMMA 10 device. It is a minimum-B anchored tandem mirror with outboard axisymmetric plug and barrier cells [5,8,9], having an axial length of $z = 27$ m, and the total volume of the vacuum vessel of 150 m^3. The central cell has a length of 6 m and a limiter with a diameter of 36 cm, and the magnetic-field intensity at the midplane $B_z = B_m$ is 0.405 T with a mirror ratio R_m of 5.2. Ion-cyclotron heatings (ICH) (200 kW at 4.47 or 6.36 MHz, as well as 100 kW at 9.9 or 10.3 MHz) are employed for the central-cell hot-ion production and the anchor stabilization, respectively [19,20]. The plug and barrier cells are axisymmetric mirrors; they have an axial length of 2.5 m ($B_m = 0.497$ T, and $R_m = 6.2$). Microwaves at 28 GHz are injected in the extraordinary mode into the plug and the barrier regions to produce ϕ_c and a thermal-barrier potential ϕ_b, respectively. Absolute values of Φ_P are measured with our originally developed electrostatic end-loss ion-energy spectrometer (IES) arrays [21]. Barrier potentials Φ_B and Φ_C are directly measured with heavy-ion (Au^0) beam probes (HIBP) [22]. Therefore, one can obtain ϕ_c and ϕ_b as $\Phi_P - \Phi_C$ and $\Phi_C - \Phi_B$, respectively.

In Fig. 2(a), the central-cell line density nl_c of a hot-ion mode plasma with $T_i = 4$ keV increases during plug ECH in association with reducing fluctuations. Various fluctuation diagnostics, including a movable microwave interferometer, the Fraunhofer-diffraction method [23], two sets of developed 50-channel soft x-ray detectors using microchannel plates [9,10,24] in the central-cell midplane, eight Langmuir probes (i.e., every 45° at $r_c = 18$ cm in the central cell) for wave phasing and coherence diagnostics [20], the above-described HIBP [22], and eight sets of IES (for more detail, see Ref. [21]), as well as simultaneous potential diagnostics with HIBP and IES, show consistently the same characteristic features as described below.

At first, two data sets, one before [Figs. 2(b)–2(f)] and one during [Figs. 2(g)–2(k)] ECH ($P_{\text{ECH}} = 180$ kW), are compared. Frequency analyses of IES signals, for instance, are shown in Fig. 2(b). The existence of electron drift waves with the *coherent* mode numbers $m = 1, 2, \ldots$ [20,23], giving a peaked structure (see arrows) over a few kHz [23], and broadband *turbulent fluctuations* having *incoherent* azimuthal phase relations are found. In Figs. 2(e) and 2(j), W_r deduced from measurements of the density profile and Φ_C with IES and HIBP is plotted. It is found that a weak shear is formed in the case without ECH [Fig. 2(e)]. On the other hand, a data set during ECH [Figs. 2(g)–2(k)] having a stronger shear [Fig. 2(j)] shows a significant difference. Figures 2(h) and 2(i) show a considerable reduction of fluctuations over all radii, and particularly near the plasma axis and $r_c \approx 10$ cm, where the shear has the maximal values. Nevertheless, an appreciable level of fluctuations still exists at about $r_c = 6$–7 cm, where no shear is formed. [Here, for reference, both E_r shear and W_r values are plotted (see above).]

In Figs. 2(m)–2(q), a similar data set to that in Figs. 2(b)–2(f) having turbulence is obtained, although ECH ($P_{\text{ECH}} = 120$ kW) is applied in Figs. 2(m)–2(q) as in Figs. 2(g)–2(k). However, remarkably different behavior is found in these two data sets. As one can see in Fig. 2(p), a weaker shear than that in Fig. 2(j) is formed.

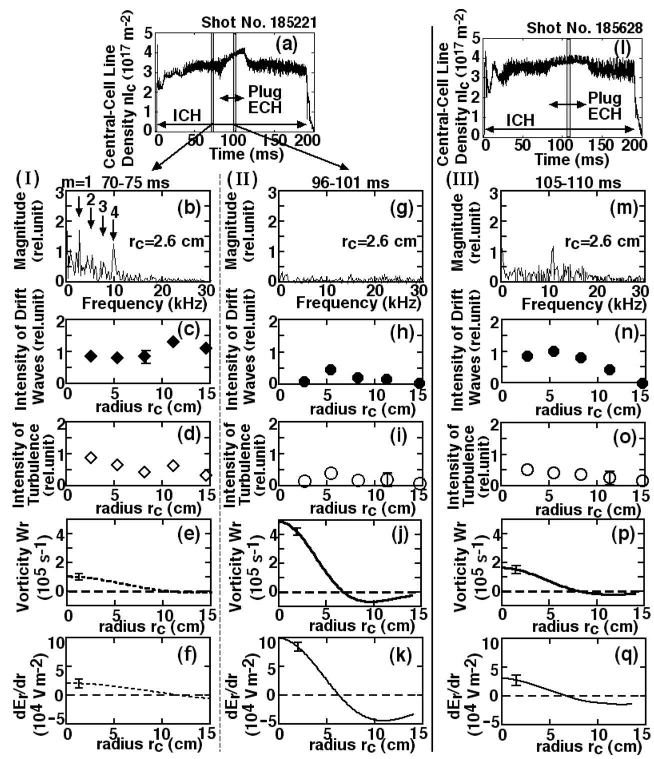

FIG. 2. Data sets of (I) ICH plasmas having a weak shear (a small W_r) (b)–(f), and (II) with plug ECH (180 kW) producing a strong shear (a large W_r) (g)–(k). In (b), Fourier components of coherent drift waves with mode numbers m (see Ref. [23]) and broadband incoherent turbulent signals for IES, for instance, are suppressed in (g)–(k) except at $r_c \approx 6$–7 cm having approximately zero shear. (III) Another data set during weaker plug ECH (120 kW) in (l)–(q) having a weaker shear as compared to that in (g)–(k). Noisier and earlier saturated density rise in (l) during ECH is found in comparison to that in (a).

For this weak shear, a lower-level saturation of density rise is found during ECH [Fig. 2(l)] with stronger density fluctuations [compare nl_c in Fig. 2(a) during ECH].

The difference in the density rise in Figs. 2(a) and 2(l) is carefully investigated by the use of a widely employed particle-balance equation, $edN/dt = I_s - I_\parallel - I_\perp$ [1,4,5,9,12,23]. Here, the contribution of nonambipolar $I_\perp$ to total $I_\perp$ is observed to be ignorable as compared to ambipolar $I_\perp$ by using floated end plates having $\approx M\Omega$ resistance (for more details, see Ref. [25]). In Fig. 3(a), a rising rate edN/dt of the total particle number N during ECH [see Fig. 2(a)] integrated along a specific axial flux tube well balances the difference between particle source currents I_s deduced from H_α detector-array data and an axial-loss current $I_\parallel$ from IES placed along the corresponding flux tube (for more details, see Refs. [1,5,12,23]). It is noted that $I_\parallel$ is obtained from the envelope of "saw-toothed" end-loss signals in Fig. 3(b) because of a sinusoidal ion-repeller biasing for IES [21]. This shows negligible $I_\perp$. The property of $I_\parallel \gg I_\perp$ is consistently confirmed by good agreement between the data on $I_\parallel$ in Fig. 3(b) and Pastukhov's theoretically evaluated $I_\parallel$ [filled circles in Fig. 3(b)], since the Pastukhov theory [7] predicts $I_\parallel$ under the assumption of negligible $I_\perp$.

On the other hand, the data in Figs. 3(c) and 3(d) correspond to the data set in Figs. 2(l)–2(q). By the use of the same methods, an appreciable amount of $I_\perp$ [see diamonds in Fig. 3(c) during ECH, as compared with those in Fig. 3(a) during ECH] is found; for instance, $I_\perp \approx (1/2)I_\parallel$ at $t = 100$ ms in Fig. 3(c). It is also noted that $I_\parallel$ observed at $t = 100$ ms in Fig. 3(d) ranges consistently about 2/3 of Pastukhov's predicted $I_\parallel$. The remainder of 1/3 of the predicted $I_\parallel$ is interpreted by the radial losses $I_\perp$ before the axial-loss currents reach mirror-end regions. This is consistent with the fact of an earlier saturation of nl_c in Fig. 2(l) in comparison to its continuous rise in Fig. 2(a) during ECH having a strong shear. Similar behavior is also found before ECH [at $t = 75$ ms in Fig. 2(a)] associated with drift waves and turbulent signals [Figs. 2(b)–2(f)] having a weak shear. Again, the particle balance requires an appreciable $I_\perp$ [Fig. 3(a)] along with disagreement between the predicted $I_\parallel$ and the data on $I_\parallel$ in Fig. 3(b).

For identifying the spatial behavior and structure of turbulence signals [Fig. 2(b)] with a weak shear [Figs. 2(e) or 2(p)], in comparison to those with a strong shear [Fig. 2(j)], contours of the central-cell soft x-ray brightness I_{sx} are shown in Figs. 4(a) and 4(b). "Hot-colored" regions indicate higher plasma-pressure locations. One can find spatially and temporally varied turbulent vortexlike structures during a weaker shear period [Fig. 4(b)] in the absence of ECH [Figs. 2(b)–2(f)]. These turbulent structures are, however, going to clear up

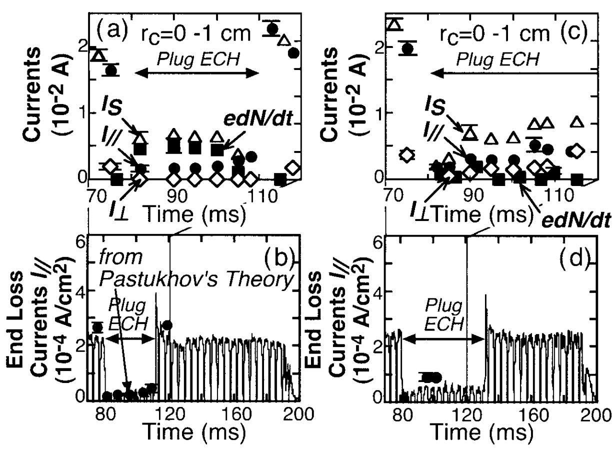

FIG. 3. Improved confinement having a strong shear during ECH in Figs. 2(g)–2(k) is analyzed from (a) a particle-balance equation; no appreciable transverse loss $I_\perp$ and consistently good agreement with (b) Pastukhov's predicted $I_\parallel$ (filled circles) are found. On the other hand, poor confinement with a weak shear [Figs. 2(l)–2(q)] is accompanied by an appreciable $I_\perp$ in (c). [Here, $I_\perp = (1/2)I_\parallel$ at $t = 100$ ms in (c), for instance.] Also, $I_\parallel$ at $t = 100$ ms in (d) is consistently about 2/3 of Pastukhov's predicted $I_\parallel$. The remainder of $I_\parallel$ is interpreted by $I_\perp$ before reaching mirror ends. This is consistent with an earlier saturation of nl_c in Fig. 2(l) as compared to its continuous rise in Fig. 2(a) during ECH with a strong shear.

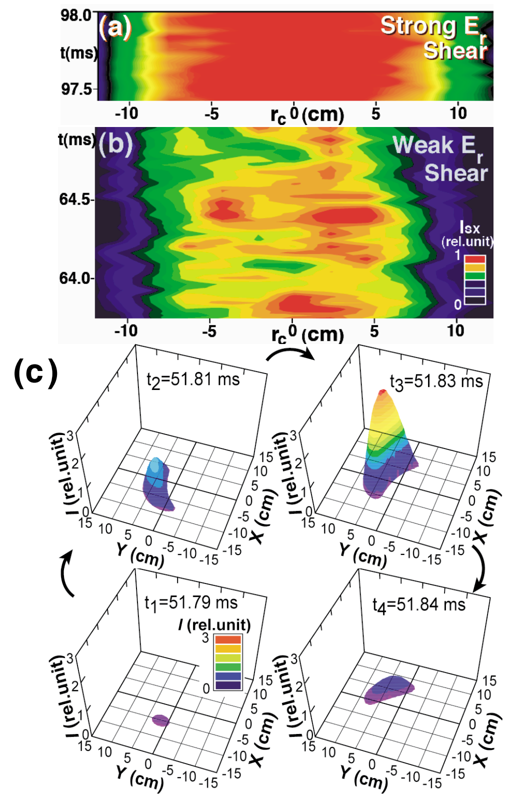

FIG. 4 (color). Contours of central-cell x-ray brightness in the cases with (a) strong and (b) weak E_r shear formation. "Hot-colored areas" show higher plasma-pressure locations. Vortexlike structures are found in (b). The temporal evolution of a vortex is exemplified in (c) by the use of our developed x-ray tomography systems. ($I \propto n_e n_i T_e^{2.3}$.)

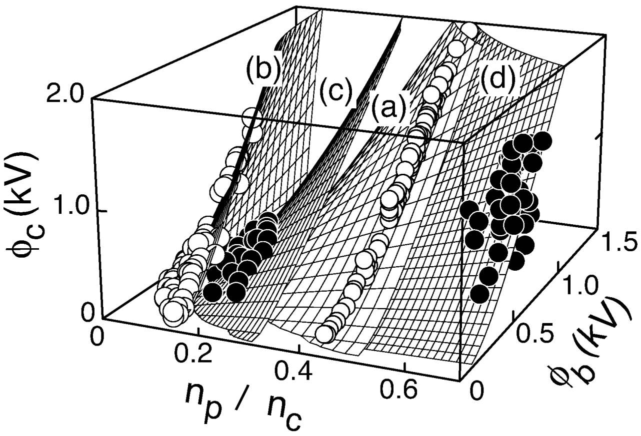

FIG. 5. The validity of theoretical surfaces for potential formation [16] covering (a) the high-potential and (b) hot-ion modes is extensionally investigated by using the advanced data for constructing potential physics interpretations and controlling potential enhanced E_r shear. Data well fit to surfaces (c) and (d) for the modes of (b) and (a) with central ECH, respectively, along with (d) plug NBI.

with ECH [Fig. 4(a)] together with the simultaneous disappearance of the broadband Fourier component [compare Fig. 2(b) with Fig. 2(g)] as well as a temperature rise [Fig. 4(a)]. A combination of x-ray data from the above-described detector array and another one having a 135° separation in the central midplane allows us to reconstruct a detailed vortex structure [Fig. 4(c)]. Its typical lifetime from formation to disappearance ranges 100 μs with a rotational motion of an $E_r \times B_z$ drift approximately. In Fig. 4(c), the center of the vortexlike structure appears at $r_c \approx 5$ cm and is faded at $r_c \approx 7$ cm into a detector noise level. Consequently, the existence of such vortexlike turbulent phenomena may provide a correlation with the appearance of the above-described additional transport $I_\perp$ with confinement degradation [Figs. 3(c), 3(d), and 4(b)] in the case with a weak shear formation, while these turbulence phenomena disappear and confinement is improved with a strong shear formation [Figs. 3(a), 3(b), and 4(a)]. From a common physics viewpoint, such investigations by using easy controllability of E_r shear in mirror devices may provide an opportunity for exploring extended and generalized cooperation researches related to the mechanism identification of the H-mode pedestal, the blob, and the internal transport-barrier formation [26].

Finally, for constructing physics interpretations and control methods of such potential and the associated E_r shear formation, the validity of our proposed potential mechanism [16] for (a) the high-potential and (b) hot-ion modes is extensionally tested in Fig. 5. The surfaces in Fig. 5 are calculated from the strong ECH theory (plateau formation) [6] in combination with the generalized Pastukhov's theory on energy confinement [7] (for more detail, see Ref. [16]). Central ECH, increasing electron axial flows from the central cell into the plug regions over ϕ_b, provides an increase in the density ratio of the plug to central regions, n_p/n_c. In Fig. 5, as found on the surfaces (c) and (d) with central ECH along with (d) additional plug neutral beam injections (NBI), the validity is still confirmed under these auxiliary-heating conditions.

In summary, three-time progress in the formation of ϕ_c including a record of 2.1 kV is achieved in the hot-ion mode in comparison to ϕ_c attained 1992–2002 [14,15] (Fig. 1). The advance in the potential formation leads to a finding of remarkable effects of a strong E_r shear or W_r on the suppression of not only coherent drift waves but also vortexlike turbulent fluctuations (Figs. 2 and 4) in association with confinement improvement (Fig. 3). The progress in the potential formation is made in line with the extension of proposed physics scalings [16] (Fig. 5).

[1] R. F. Post, Nucl. Fusion **27**, 1579 (1987), a review paper of mirrors; Trans. Fusion Sci. Technol. **43**, 195 (2003).
[2] D. D. Ryutov, in *Proceedings of the International Conference on Plasma Physics, New Delhi, 1989* (IAS, Bangalore, 1989).
[3] A. C. England *et al.*, Trans. Fusion Sci. Technol. **43**, 73 (2003); M. Kwon *et al.*, *ibid.* **43**, 23 (2003).
[4] N. Hershkowitz, S. Miyoshi, and D. D. Ryutov, Nucl. Fusion **30**, 1761 (1990).
[5] S. Miyoshi *et al.*, Fiz. Plazmy **23**, 781 (1997) [Plasma Phys. Rep. **23**, 723 (1997)].
[6] R. H. Cohen, Phys. Fluids **26**, 2774 (1983).
[7] V. P. Pastukhov, Nucl. Fusion **14**, 3 (1974); R. H. Cohen *et al.*, Nucl. Fusion **18**, 1229 (1978); **19**, 1295 (1979); **19**, 1693 (1979).
[8] T. Cho *et al.*, Phys. Rev. Lett. **64**, 1373 (1990).
[9] T. Cho *et al.*, Phys. Rev. A **45**, 2532 (1992).
[10] T. Cho *et al.*, Nucl. Fusion **27**, 1421 (1987).
[11] T. Kariya *et al.*, Phys. Fluids **31**, 1815 (1988).
[12] T. Cho *et al.*, Nucl. Fusion **28**, 2187 (1988).
[13] T. Cho *et al.*, Nucl. Fusion **41**, 1161 (2001).
[14] T. Cho *et al.*, in *Proceedings of the 19th IAEA Fusion Energy Conference, Lyon, 2002* (IAEA, Vienna, 2003).
[15] T. Cho *et al.*, Nucl. Fusion **43**, 293 (2003).
[16] T. Cho *et al.*, Phys. Rev. Lett. **86**, 4310 (2001).
[17] Y. Kiwamoto *et al.*, Phys. Plasmas **3**, 578 (1996).
[18] A. V. Timofeev, *Review of Plasma Physics* (Consultants Bureau, New York, 1992), Vol. 17, pp. 193–301.
[19] M. Ichimura *et al.*, Nucl. Fusion **39**, 1995 (1999).
[20] S. Tanaka *et al.*, Rev. Sci. Instrum. **70**, 979 (1999).
[21] M. Yoshida *et al.*, Rev. Sci. Instrum. **74**, 1909 (2003).
[22] K. Ishii *et al.*, Rev. Sci. Instrum. **60**, 3270 (1989).
[23] A. Mase *et al.*, Phys. Rev. Lett. **64**, 2281 (1990); Nucl. Fusion **31**, 1725 (1991).
[24] M. Hirata *et al.*, Nucl. Instrum. Methods Phys. Res., Sect. B **66**, 479 (1992).
[25] I. Katanuma *et al.*, Nucl. Fusion **27**, 2041 (1987).
[26] Y. Kishimoto *et al.*, Nucl. Fusion **40**, 667 (2000), and references therein.